International Journal of Multiphysics
Volume 18, No. 3, 2024
ISSN: 1750-9548

Theoretical Analysis of Structural, Electronic, and Optical Properties of $CdXAs_2$ (X = Ge and Sn) Compounds

Khaled Lazar[1], Yousra Megdoud[2,3], Redha Meneceur[1], Yamina Benkrima[4] and Latifa Tairi[5]

[1] UDERZA Unit, Faculty of Technology, University of El-Oued, Algeria.
[2] Institute of Sciences, University Center of Tipaza, Algeria.
[3] LPR Laboratory, Department of Physics, Faculty of Science, Badji Mokhtar University, Annaba, Algeria.
[4] Ecole Normale Superieure de Ouargla 30000 Algeria
[5]Research Center in Industrial Technologies CRTI, P.O. Box 64, Cheraga16014 Algiers, Algeria.
correspondant Author : b-amina1@hotmail.fr

Submitted: 03/10/2024 Revised: 27/12/2024 Accepted: 10/01/2025

Abstract:

A first-principles investigation has been conducted to explore the structural, electronic, optical properties of chalcopyrite $CdXAs_2$ (X = Ge, Sn) using density functional theory (DFT). The calculations were performed within the full-potential linearized augmented plane wave (FP-LAPW) method, employing both WC-GGA and mBJ-GGA approximations for the exchange-correlation potential. The study thoroughly examines the impact of cation substitution (Ge or Sn) on various fundamental properties, including lattice parameters, electronic band structure and optical characteristics. The influence of structural modifications on the energy band gap has been analyzed in detail, along with the evaluation of key optical parameters such as the dielectric function, refractive index, and absorption coefficient, which are crucial for determining the potential of these compounds in optoelectronic applications. The results demonstrate strong agreement with previously reported theoretical and experimental data. This study underscores the significance of $CdXAs_2$ materials in advanced nanotechnology and electronics, paving the way for further investigations into structural modifications and elemental substitutions to enhance their functional properties.

Keywords: DFT; chalcopyrite; bandgap; Optical properties; photovoltaic .

1. Introduction

The increasing global energy demand and environmental concerns have driven extensive research into sustainable energy solutions. Among these, solar energy conversion stands out as one of the most promising alternatives to fossil fuels. Solar power is considered an inexhaustible resource on a human timescale, making it a clean and renewable energy source that does not contribute to environmental degradation. To efficiently harness solar energy, the development of advanced semiconductor materials with optimal optoelectronic properties is essential. Semiconductor compounds belonging to the $I\text{-}III\text{-}VI_2$ and $II\text{-}VI\text{-}V_2$ families **[1-5]** have emerged as strong candidates for photovoltaic applications due to their suitable bandgaps and high absorption coefficients in the visible spectrum (approximately 10^5 cm^{-1}). Among these materials, $CdXAs_2$ (X = Ge and Sn) compounds belong to the $I\text{-}III\text{-}VI_2$ class, which can be derived from binary II-VI semiconductors such as ZnS, which crystallize in a zinc blende structure. The ordered substitution of Zn cations by Cu (group I) and X (group III: Al, Ga, In) leads to structural modifications, transforming the symmetry from cubic to tetragonal, with a space group $\bar{I}42d$. **[6]** This structural change also affects the lattice parameter ratio (c/a), which typically approaches or slightly deviates from 2 in most cases. The anisotropic nature of these compounds results in birefringence, which plays a crucial role in their optical behavior. This birefringence enables phase-matching conditions by angular tuning, making these materials highly relevant for laser applications, such as CO_2 lasers. In high-altitude regions, where solar radiation remains intense and nearly four times stronger than at the Earth's surface, high-power lasers based on $CdXAs_2$ compounds **[7-9]** could be deployed in geostationary orbits to capture and redirect solar energy toward terrestrial photovoltaic systems. Such an approach minimizes lateral dispersion and enhances energy transmission

efficiency. Previous Studies and Research Gaps several theoretical investigations have explored the electronic and optoelectronic properties of $CdXAs_2$ compounds. For instance, Zhang Xian-Zhou analyzed their band structure using the Perdew-Burke-Ernzerhof (PBE-GGA) exchange-correlation functional. Similarly, Anima Ghosh employed the Tran-Blaha modified Becke-Johnson (mBJ-GGA) approach to refine electronic bandgap predictions. Other studies, such as those by Wenfeng Li et al. and Xue Li et al., have examined the electronic and thermoelectric behavior of these materials using the mBJ-GGA method. Additionally, Bodnar experimentally characterized the thermal properties of the $CdXAs_2$ system.

Despite these valuable contributions, certain crucial aspects of $CdXAs_2$ compounds remain insufficiently explored. Notably, comprehensive studies on the optoelectronic properties of $CdGeAs_2$ and $CdSnAs_2$, particularly their birefringence behavior, are lacking. Our work addresses this gap by providing the first theoretical estimation of birefringence in these materials. Unlike prior studies that primarily focused on electronic properties, we emphasize the impact of X-cation substitution (X = Ge and Sn) on structural, electronic, and optical characteristics**[10,11]**. A deeper understanding of these properties is essential for optimizing these materials for photovoltaic and other optoelectronic applications. Moreover, thermal properties have received little attention in previous computational studies. **[12-18]** Apart from the work by Sheetal Sharma et al**[19]**. on $CdGeAs_2$ and $CdSnAs_2$, first-principles calculations of thermal behavior remain scarce. Understanding thermal properties is crucial for assessing material stability under varying pressure and temperature conditions**[20]**, particularly where experimental data are unavailable. **[21]** These calculations also provide insights into optimizing crystal growth conditions, ensuring high-quality synthesis of these semiconductors for practical applications. Objective of the Study is : The primary goal of this research is to bridge the existing knowledge gaps by conducting a comprehensive first-principles investigation of $CdXAs_2$ compounds (X = Ge and Sn). Using density functional theory (DFT) within the full-potential linearized augmented plane wave (FP-LAPW) method, we systematically analyze their structural, electronic, optical, and thermal properties. Our study aims to examine the impact of X-cation substitution on structural parameters and electronic band structure and evaluate optical properties, including birefringence and phase-matching conditions, to assess their suitability for laser and photovoltaic applications. Analyze thermal characteristics, particularly under varying temperature and pressure conditions, to optimize material performance in extreme thermodynamic environments. Compare theoretical predictions with available experimental data, ensuring consistency and reliability of the findings. By addressing these aspects, our work aims to provide valuable insights for future experimental developments and practical applications of $CdXAs_2$ compounds in advanced optoelectronic and energy conversion technologies.

2. Details of Calculations

To comprehensively investigate the structural, electronic, and optical properties of $CdXAs_2$ (X = Ge and Sn), we employed **first-principles calculations** based on **density functional theory (DFT) [22]**. These calculations were carried out using the **Full-Potential Linearized Augmented Plane Wave (FP-LAPW) method**, **[23]** as implemented in the **WIEN2k [24] computational package**. The FP-LAPW approach is well-regarded for its high accuracy in solving the **Kohn–Sham equations**, **[25]** enabling an all-electron, full-potential treatment of complex crystalline systems.

The exchange-correlation (XC) energy, a crucial component in DFT calculations, was treated using the **Wu–Cohen Generalized Gradient Approximation (WC-GGA)**. **[26]** .This functional is known for its improved accuracy in predicting structural and thermodynamic properties compared to conventional GGA approaches. However, since standard GGA functionals tend to underestimate bandgap values, a **hybrid approach** was adopted. To refine the electronic band structure calculations and obtain more reliable bandgap estimates, we incorporated the **Tran–Blaha modified Becke–Johnson (TB-mBJ) exchange potential**, **[27]** combined with GGA for the correlation term. This approach has been shown to significantly enhance bandgap predictions, making them comparable to experimental values.

In our computational framework, the unit cell was systematically divided into two regions:

1. **Interstitial Region (IR):** The space between atomic spheres, where wavefunctions were expanded in terms of plane waves to capture electronic behavior with high accuracy.

2. **Muffin-Tin (MT) Spheres:** These non-overlapping atomic spheres were centered around individual atomic positions, with wavefunctions expanded using a linear combination of atomic-like wave functions and spherical harmonics.

To ensure a rigorous treatment of charge density and potential across the unit cell, specific truncation parameters for spherical harmonics were carefully chosen:

- **RMT × Kmax = 8**, where **Kmax** is the maximum reciprocal lattice vector within the first Brillouin zone, and **RMT** is the smallest muffin-tin radius.

- **Maximum angular momentum value lmax = 10**, ensuring a comprehensive expansion of the wavefunctions within the MT spheres.

- The **Fourier expansion of the charge density** was set to **Gmax = 12 (Ry)$^{1/2}$**, ensuring a high level of precision in potential and total energy calculations.

- **Total energy convergence threshold below 10^{-4} Ry**, ensuring stable and precise results.

The combination of **WC-GGA and TB-mBJ [28]** functionals, along with the **FP-LAPW method**, provides a highly reliable computational approach for investigating the structural, electronic, and optical properties of $CdXAs_2$ compounds. The rigorous treatment of **relativistic effects, charge density expansion, and k-point sampling** ensures that our findings offer valuable insights into the material's potential applications in **photovoltaics and optoelectronics. [29,30]**

3. Results and Interpretations

3.1. Structural Properties

This section focuses on analyzing the **structural characteristics** of the studied compounds, **$CdGeAs_2$ and $CdSnAs_2$**. These materials belong to the **I-III-VI_2 family**, which exhibits a unique **superlattice arrangement derived from the ZnS phase**. The structural transformation from ZnS occurs through a systematic **cationic substitution mechanism**, where: **Group II elements in ZnS (e.g., Zn ions) are replaced by Group I transition metal ions** such as **Cd**. **Group III elements**, **[31]** which are commonly found in semiconductors, replace the remaining cations. As a consequence of this substitution, each anion (**As**) (**Figure 1**)forms a tetrahedral coordination with **two Cd ions and two Ge and Sn cations**, resembling the fundamental atomic arrangement of ZnS.

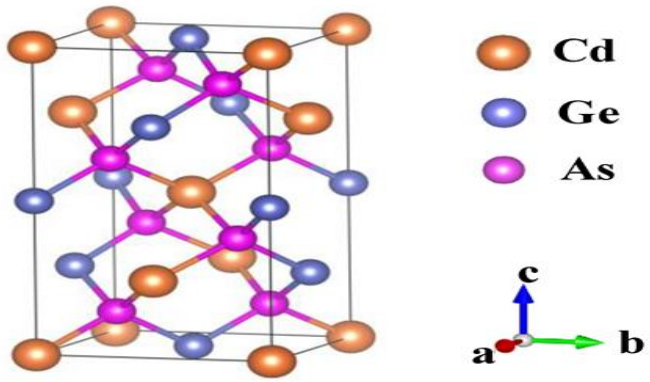

Figure 1. Exemple of Crystalline structure of $CdGeAs_2$.

However, compared to the ideal **zinc-blende structure**, **[32]** the systematic replacement of **Ge and Cd cations** introduces **two primary structural distortions**: Firstly, **Tetragonal Distortion (η = c/2a)** One major structural deviation is a **tetragonal distortion** along the (001) crystallographic direction. This distortion is quantified by the parameter **η = c/2a**, where **η deviates from unity**, indicating an elongation or compression of the lattice along this axis. This effect arises due to the **mismatch in ionic radii** between **Cd and Ge cations**, which disrupts the perfect cubic symmetry of the original ZnS phase. Secondly, **Tetrahedral Distortion and Bond Length Variation.** Another key modification results from the emergence of **two distinct chemical bonds** with **unequal bond lengths** within the tetrahedral framework. This phenomenon, often referred to as **tetrahedral distortion**, is driven by the displacement of **Te and Se atoms** from their **ideal tetrahedral positions [32]** at **(1/4, 1/4, 1/4)**. This displacement introduces an additional **internal degree of freedom**, represented by the **u parameter** in the chalcopyrite phase. Unlike in the **zinc-blende structure**, where **u remains fixed at 0.25**, this parameter varies based on **the internal positioning of Ge and As anions [33,34]**, further affecting the material's electronic and optical properties. Due to these distortions, the **crystal symmetry transitions** from the **zinc-blende space group F$\bar{4}$3m** to the **chalcopyrite space group I$\bar{4}$2d**. Within this **chalcopyrite configuration**, the atomic positions of **Cd, Ge, Sn and As** are defined as **(0,0,0), (0,0,0.5), and (u,0.25,0.125)**, respectively.

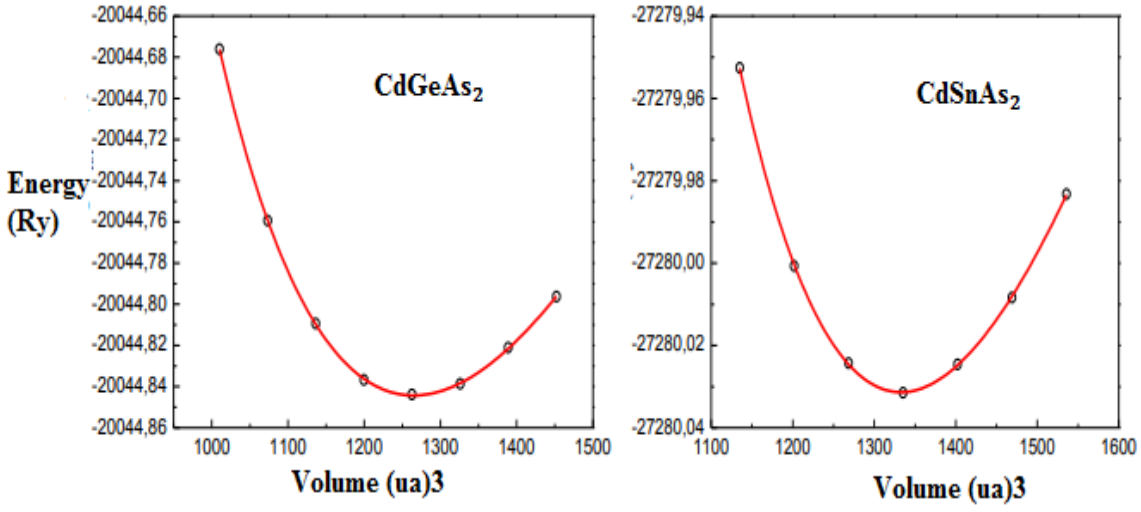

Figure 2 : Total energy versus volume calculated for compounds **$CdGeAs_2$** and **$CdSnAs_2$.**

Computational Approach for Structural Optimization to determine the equilibrium structure al parameters of $CuInSe_2$ and $CuInTe_2$, calculations were performed using the WIEN2K package [17,20], following a multi-step optimization procedure: Energy vs. Volume Optimization, the total energy was computed as a function of volume, keeping the c/a ratio constant, to establish the equilibrium volume. c/a Ratio Optimization. The c/a ratio was then optimized by analyzing its energy dependence, while maintaining the previously determined equilibrium volume.. Tetrahedral Parameter "u" Optimization. The internal parameter "u" was minimized using the Mini procedure implemented in WIEN2k **[25],** ensuring precise determination of atomic positions. After performing these optimization steps, the final equilibrium structural parameters were obtained, and the resulting total energy vs. volume curve was plotted (see Figure 2).

Table1. The Structural Optimization of $CdGeAs_2$ and $CdSnAs_2$.

	Parameter	**This Work**	**Experimental Value [16] [21]**	**Relative Error**
$CdGeAs_2$	**a=b (A^0)**	**5.94**	**5.94**	**1.72**
	c= (A^0)	**11.72**	**11.22**	**1.72**
	C/a	**1.97**		

$CdSnAs_2$	**a=b= (A^0)** **c= (A^0)** **C/a**	**6.22** **12.45** **2.001**	**-**	**1.82** **1.82**

3.2. Electronic Properties and Band Structure Analysis

This section provides an in-depth analysis of the **electronic properties** of **$CdGeAs_2$ and $CdSnAs_2$** with a particular emphasis on their **energy band structures**. The band structures were computed along **high-symmetry paths within the first Brillouin zone**, utilizing both the **WC-GGA (Wu-Cohen Generalized Gradient Approximation) and the mBJ (modified Becke-Johnson) exchange potential**. As a representative example, **Figure 3** presents the calculated band structures for both compounds.

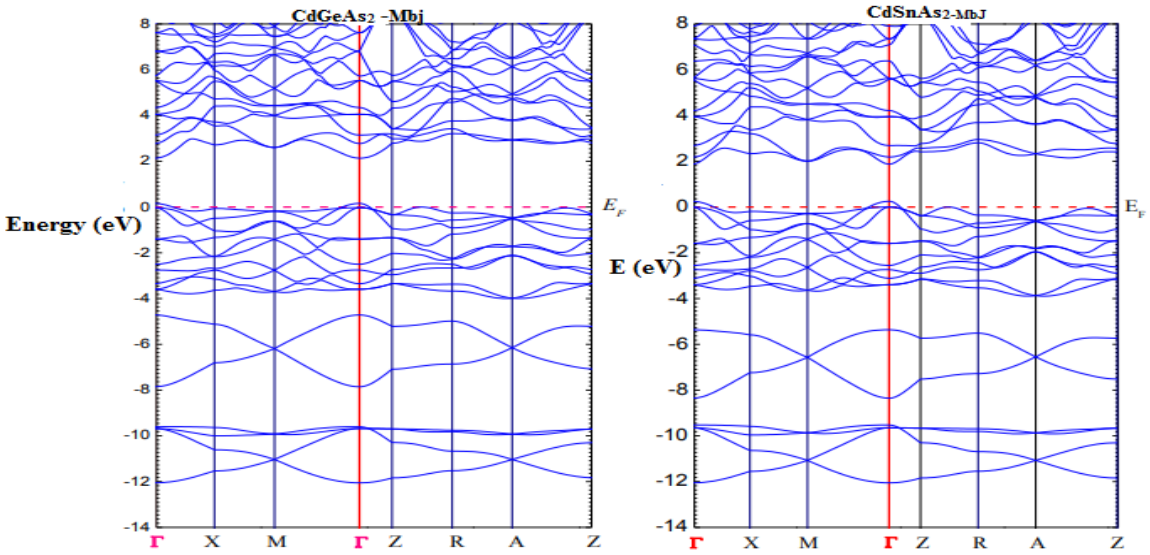

Figure 3. Calculated band structures of $CdGeAs_2$ and $CdSnAs_2$ compounds using the mBJ approximation.

A- Direct Bandgap Nature and Key Observations

A significant observation across both materials is that the **valence band maximum (VBM) and conduction band minimum (CBM) are both located at the Γ point**, confirming a **direct bandgap** nature for **$CdGeAs_2$ and $CdSnAs_2$**. The direct transition characteristic is crucial for optoelectronic applications, as it enhances the efficiency of light absorption and emission processes. The precise values of the calculated bandgaps are listed in **Table 2**, allowing for a comparative analysis against previous **theoretical predictions and experimental measurements [12-16].**

Table2. Band gap value E_g for $CdGeAs_2$ and $CdSnAs_2$.

	E_g (eV)		
Compounds	**mBj**	**WC-GGA**	**Ref [12] [16] [21]**
$CdGeAs_2$	**0.79**	**0.531**	**0.67**

			0.69
$CdSnAs_2$	**0.494**	**0.122**	**0.26**

B- Comparison of WC-GGA and mBJ Approximations

The computed **electronic band structures using the mBJ method** exhibit **qualitative similarity** to those obtained via **WC-GGA**. However, the key distinction lies in the **quantitative accuracy** of the bandgap values:

- The **mBJ approach significantly improves bandgap predictions**, yielding values **much closer to experimental results** compared to **WC-GGA**.
- This enhancement stems from **mBJ's refined treatment of exchange interactions**, effectively reducing the well-known **underestimation of bandgaps** inherent in standard GGA-based functionals.
- The **mBJ potential** incorporates a **semi-local orbital-dependent exchange correction**, leading to **better bandgap accuracy without the computational cost of hybrid functionals [26].**

For further refinement, hybrid functionals such as **B3PW91 [27]** incorporate a **fraction of nonlocal Hartree-Fock (HF) exchange**, mitigating self-interaction errors. However, these functionals demand significantly **higher computational resources** compared to the **semi-local mBJ potential**. **Bandgap Reduction Trend from $CdGeAs_2$ to $CdSnAs_2$**

One of the most striking trends observed in the band structure analysis is the **systematic decrease in bandgap energy when transitioning from $CdGeAs_2$ to $CdSnAs_2$**. This trend aligns well with **experimental findings [12-16]** and can be attributed to multiple factors: **Lattice Parameter Expansion,** The substitution of **Te** for **Se** leads to an **increase in lattice parameters (a, c)**, resulting in a **lower bulk modulus (B)**. This expansion **weakens the bonding interactions**, subsequently reducing the **energy separation between the valence and conduction bands**, thus **narrowing the bandgap**. These structural and chemical factors collectively contribute to the **observed reduction in bandgap energy**, reinforcing the crucial interplay between **crystal structure, bonding characteristics, and electronic properties**. The graphical representation of these trends in **Figure 3** further illustrates the connection between **structural modifications and electronic behavior**.

3.3. Optical Properties

The optical properties of solid materials offer valuable insights into the **fundamental interactions between electromagnetic waves and the electronic and ionic components** of a system. At the microscopic scale, these interactions can be described with precision. However, to provide a **macroscopic and quantitative understanding**, the **dielectric function ε(ω)** plays a crucial role. It is mathematically expressed as**: $\varepsilon(\omega) = \varepsilon 1(\omega) + i\varepsilon 2(\omega)$ [35-37].**

where **$\varepsilon_2(\omega)$** is associated with **electronic transitions**, governing the absorption mechanisms within the material. This component is computed by analyzing the **momentum matrix elements** connecting occupied and unoccupied electronic states **[38].** Meanwhile, **$\varepsilon_1(\omega)$** is directly related to **polarization effects** and is determined from **$\varepsilon_2(\omega)$** using the well-established **Kramers-Kronig relations [33,34].** By leveraging these mathematical relationships, one can derive other critical optical parameters, including the **absorption coefficient α(ω)** and the **refractive index n(ω)**, both of which provide essential information regarding the optical response of the material. This study aims to **analyze the optical properties of $CdGeAs_2$ and $CuSnAs_2$** using the **modified Becke-Johnson (mBJ) potential**. The goal is to **enhance the understanding of their optical performance, particularly in photovoltaic and optoelectronic applications [39].** Notably, these compounds exhibit **optical anisotropy**, influenced by the **electric field orientation relative to the crystallographic axes**. To characterize this anisotropic

behavior, we distinguish between: ε_{xy} **(perpendicular component):** Represents the dielectric response when the electric field is oriented **perpendicular to the Oz axis**, averaged over the **x and y directions**. εz **(parallel component):** Corresponds to the dielectric response when the electric field is aligned **parallel to the Oz axis**. we gain deeper insights into their optical response, further reinforcing their **potential for advanced optoelectronic applications**.

3.3.1. The Real and Imaginairy Part of the Dielectric Function

Figure 4 illustrates the real part of the dielectric function, $\varepsilon_1(\omega)$, for **$CdGeAs_2$** and **$CdSnAs_2$**, spanning photon energies up to **40 eV**. The spectral profiles of these two compounds exhibit notable similarities, particularly at lower energy levels, where they display an **isotropic optical response**.

A key observation from **Figure 4** is the **gradual decrease in the energy of the primary peak** as one transitions from **$CdGeAs_2$ (1.80 eV) to $CdSnAs_2$ (1.55 eV)**. This shift in energy originates from variations in the **electronic band structure** of these materials. Additionally, **$\varepsilon_1(\omega)$ reaches zero energy in the ultraviolet region**, marking the **threshold beyond which dispersion ceases [35].** Beyond this point, the dielectric function continues to decline, dropping below **unity in the UV range** before surpassing it again at approximately **11.87 eV for $CuInSe_2$** and **15.08 eV for $CuInTe_2$**. These **critical frequencies correspond to the plasma frequency (ω1)**, aligning with the energy of the primary peak in **energy-loss spectra** [36].

Within the **energy range where $\varepsilon_1(\omega) < 0$**, electromagnetic waves **cannot propagate**, leading to a sharp increase in **reflectivity** and inducing **metallic behavior** in these materials **[37].** This distinctive optical characteristic suggests that both **$CdGeAs_2$ and $CdSnAs_2$** could serve as **effective shielding materials against high-frequency electromagnetic waves [38]. Static Dielectric Constant and its Relationship with Band Gap.** Table 3 provides a comprehensive summary of the **static dielectric properties** of the studied compounds, incorporating both **theoretical and experimental comparisons**. A crucial parameter in this analysis is **$\varepsilon_1(0)$**, which represents the **electronic contribution to the static dielectric constant**. This metric provides valuable insights into the **interaction strength between valence and conduction band electronic states** under the influence of an external electric field. Notably, an increase in **$\varepsilon_1(0)$ is observed when transitioning from $CdGeAs_2$ to $CdSnAs_2$**, correlating with the **decreasing energy gap** as **As is substituted by Ge and Sn**. This relationship follows **Penn's model**.

These results highlight the **significant role of dielectric properties in understanding the optical behavior of $CdGeAs_2$ and $CdSnAs_2$**, emphasizing their potential applications in **advanced optoelectronic and electromagnetic shielding technologies**.

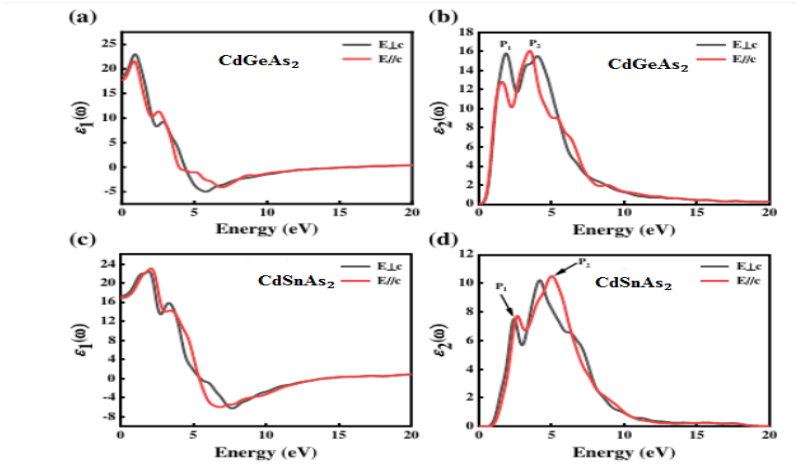

Figure 4. Calculated real and Imaginary parts of the complex dielectric constant for $CdGeAs_2$ and $CdSnAs_2$ compounds.

The imaginary part of the dielectric function, **$\varepsilon_2(\omega)$**, which is closely linked to the optical absorption processes, is depicted in **Figure 4**, covering photon energies up to **40 eV**.

In our optical calculations, **indirect band transitions were deliberately excluded**, as the influence of **phonon scattering** on dielectric screening in these cases is relatively insignificant **[43].**

A critical feature of **$\varepsilon_2(\omega)$** is the **fundamental absorption edge**, which marks the threshold where significant absorption begins. This absorption edge is observed at approximately **0.202 eV for $CdGeAs_2$** and **0.485 eV for $CdSnAs_2$**. Notably, a strong correlation emerges between the **mBJ-derived bandgap values** of these compounds and their corresponding absorption edges. This relationship is consistent with the electronic band structure, where the absorption edge aligns with the onset of **direct interband transitions at the Γ point**. These transitions involve electrons moving from the **highest occupied valence band (VB) states** to the **lowest unoccupied conduction band (CB) states**.

Beyond the **absorption threshold**, **$\varepsilon_2(\omega)$ exhibits a sharp rise**, as illustrated in **Figure 5**. This increase arises due to the **high density of interband transitions** occurring in the system. The primary peaks in **$\varepsilon_2(\omega)$** correspond to **direct transitions** between distinct energy levels within the conduction and valence bands. Interestingly, these peak positions **shift to lower energies**, specifically **5.89 eV for $CdGeAs_2$** and **1.423 eV for $CdSnAs_2$**. This downward shift in energy stems from the **differences in the electronic band structures** of the two compounds, particularly their **bandgap variations and electronic state distributions**.

These results provide **valuable insights into the optical response of $CdGeAs_2$ and $CdSnAs_2$**, reinforcing their **potential applications in optoelectronic devices, photovoltaic technologies, and electromagnetic shielding materials**.

3.3.2. The Refractive Index

The **refractive index, $n(\omega)$**, is a fundamental optical parameter that describes how light propagates through a material by quantifying its polarization response to an incident electromagnetic wave. Despite being a **macroscopic property**, it originates from the **microscopic interactions** of photons with the electronic structure of the material [45]. The refractive index is mathematically derived from the **real ($\varepsilon_1(\omega)$) and imaginary ($\varepsilon_2(\omega)$) components** of the dielectric function **[41].**

Figure 5 presents the computed refractive index **$n(\omega)$** for $CdGeAs_2$ and $CdSnAs_2$, revealing a behavior that closely follows the trend observed in **$\varepsilon_1(\omega)$**. At **low photon energies**, the refractive index exhibits **isotropic characteristics**, meaning its response is nearly identical along different crystallographic directions. This behavior is consistent with the low-energy optical response of these materials.

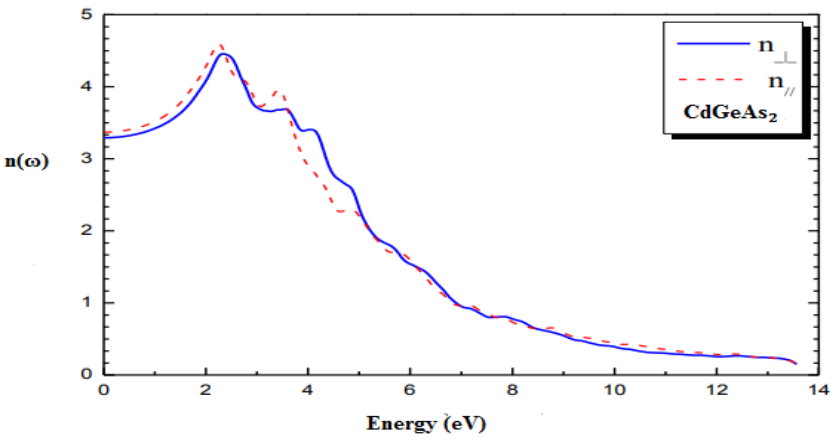

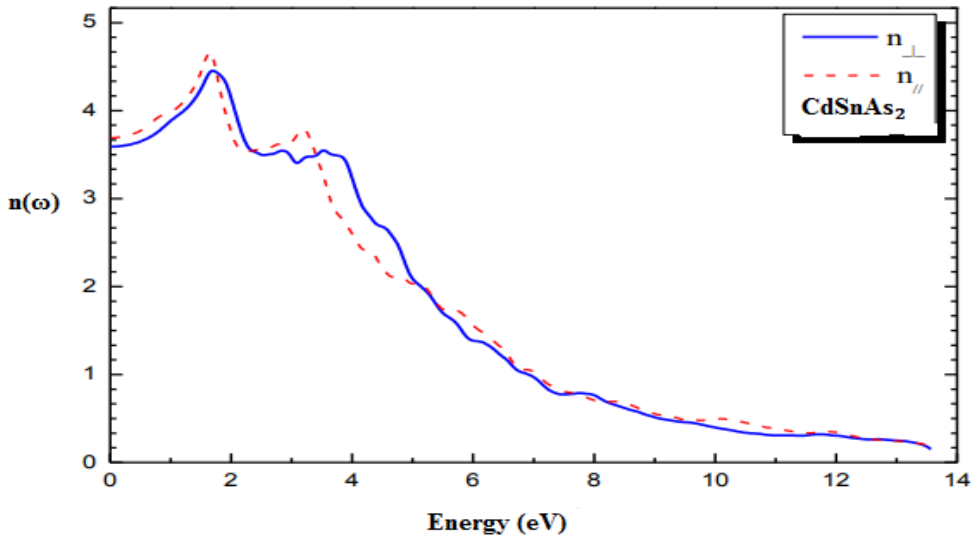

Figure 5. Variation of Refractive Index n(ω) for $CdGeAs_2$ and $CdSnAs_2$ Compounds.

The **static refractive index, n(0)**, which corresponds to the refractive index at zero frequency (long-wavelength limit), is calculated using the relation **$n(0) = \sqrt{\varepsilon_1(0)}$** [46]. The computed values for **$CdGeAs_2$ and $CdSnAs_2$ are 3.51 and 4.03**, respectively, Additionally, **n(0) exhibits a systematic increase** from $CdGeAs_2$ to $CdSnAs_2$. This trend **mirrors the variation in $\varepsilon_1(0)$** and can be attributed to the **inverse relationship between the bandgap (Eg) and the static refractive index**, as dictated by **Penn's model** [40-43]. According to this theoretical framework, a **decreasing bandgap leads to an increase in $\varepsilon_1(0)$, which in turn results in a higher refractive index**.

These findings underscore the **strong correlation between electronic structure and optical behavior** in these chalcopyrite compounds, further demonstrating their potential for applications in **photonics, optoelectronic devices, and high-efficiency solar cells**

3.3.4. Absorption Coefficient

In the field of **photovoltaic energy conversion**, the ability of a material to efficiently **absorb and convert incident radiation into charge carriers** is of paramount importance. This process, known as **photoconductivity**, is directly influenced by the **absorption coefficient ($\alpha(\omega)$)**, which quantifies how deeply light of a given wavelength can penetrate before being absorbed. The **absorption coefficient** is a critical parameter for evaluating the feasibility of materials for applications in **solar energy harvesting** and other **optoelectronic technologies** [43].

To assess the potential of **$CdGeAs_2$ and $CdSnAs_2$** for photovoltaic applications, we analyzed their absorption coefficients **up to 40 eV**, as illustrated in **Figure 6**. The absorption characteristics of these materials can be derived from the **real ($\varepsilon_1(\omega)$) and imaginary ($\varepsilon_2(\omega)$) components** of the dielectric function [43].

From **Figure 7**, the absorption edge **($\alpha(\omega)$ threshold)**—which corresponds to the **direct band gap (Eg)**—is identified at approximately **0.30 eV for $CdGeAs_2$** and **0.09 eV for $CdSnAs_2$**. This finding indicates that **$CdGeAs_2$ and $CdSnAs_2$ exhibit strong absorption in the visible spectrum**, making them highly promising materials for **solar energy conversion**.

Additionally, below the **absorption threshold**, these compounds display **high transparency and low reflectivity**, further enhancing their potential for **photovoltaic and optoelectronic applications**. The ability of

these materials to efficiently **absorb visible light while minimizing energy losses due to reflection** underscores their suitability for **next-generation solar cells** and **photodetectors**.

These insights into the **absorption properties** of $CdGeAs_2$ and $CdSnAs_2$ reinforce their **potential as efficient light-absorbing materials**, paving the way for advancements in **renewable energy and optoelectronic device engineering.**

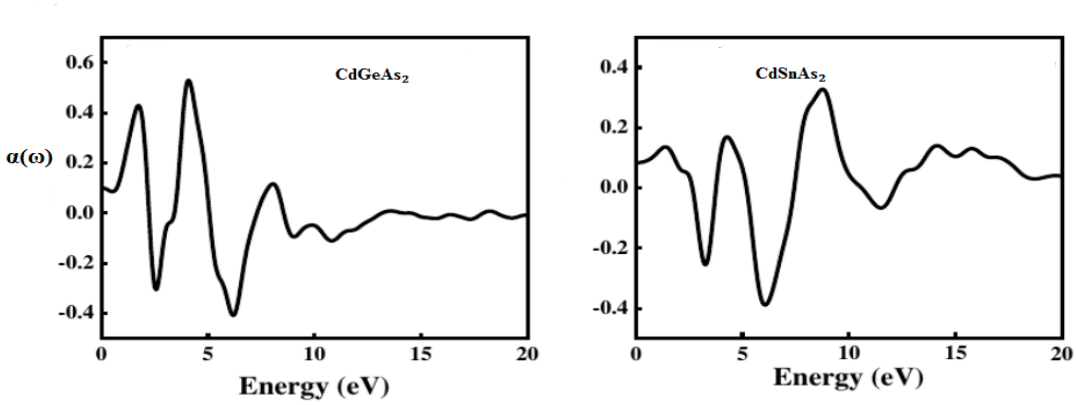

Figure 6. Calculated absorption coefficient **α(ω)** versus energy (eV) for $CdGeAs_2$ and $CdSnAs_2$ compounds.

4. Conclusion

In this study, we employed the full-potential linearized augmented plane wave (FP-LAPW) method within the WIEN2K code to conduct a comprehensive investigation of the structural, electronic, and optical properties of $CdGeAs_2$ and $CdSnAs_2$. Our findings exhibit remarkable agreement with experimental data, surpassing previous theoretical studies, particularly in the accurate prediction of band gaps, lattice parameters (a and c), and static optical properties.

A key highlight of this research is the novel analysis of birefringence, which demonstrates the potential of $CdGeAs_2$ and $CdSnAs_2$ for high-performance laser applications. This is a pioneering insight within the domain of DFT-based research, marking a significant contribution to the study of chalcopyrite materials.

Additionally, our detailed optical analysis, particularly of the absorption spectrum, underscores the exceptional potential of these compounds for photovoltaic applications within the visible range. The observed optical behavior suggests that $CdGeAs_2$ and $CdSnAs_2$ could play a crucial role in the development of next-generation optoelectronic devices, including solar cells and laser technologies.

This work provides valuable theoretical insights that can serve as a foundation for future experimental and computational studies. Further exploration of cation substitutions and doping strategies could lead to optimized materials with tailored properties for advanced optoelectronic and photonic applications.

Reference

[1] E. Rosencher, and B.Vinter, Structural Study, *Vibrational, Optical, Thermal Properties and Hirshfeld Surface Analysis of a New Iron(III) Complex Optoelectronics*, (Cambridge University Press, Cambridge, UK, (2002). https://doi.org/10.1017/CBO9780511754647

[2] A. Luque, Will we exceed 50% efficiency in photovoltaics, J. Appl. Phys. 110, 031301 (2011).https://doi.org/10.1063/1.3600702

[3] R.H. Bube, *Photovoltaic Materials*, (Imperial College Press, London, 1998). https://doi.org/10.1016/S1369-7021(07)70275-4

[4] W.N. Shafarman, and L. Stolt, in: *Handbook of Photovoltaic Science and Engineering*, edited by A. Luque, and S. Hegedus(Wiley, Chichester, UK, 2003) pp. 567–616. http://dx.doi.org/10.1002/9780470974704.ch1
[5] M.A. Green, K. Emery, Y. Hishikawa, and W. Warta, "Solar cell efficiency tables," Prog. Photovolt: Res. Appl. 18, 346-352(2010). https://doi.org/10.1002/pip.1021
[6] S. Siebentritt, and U. Rau, editors, *Wide-Gap Chalcopyrites*, (Springer, Berlin, Heidelberg, Germany, 2006).https://link.springer.com/chapter/10.1007/3-540-31293-5_9
[7] F. Chiker, B. Abbar, A. Tadjer, S. Bresson, B. Khelifa, and C. Mathieu, "Electronic structure and optical properties of ternaryCdXP2 semiconductors (X = Si, Ge and Sn) under pressure," Physica B, 349, 181-191 (2004).https://doi.org/10.1016/j.physb.2004.03.087
[8] F. Chiker, B. Abbar, A. Tadjer, S. Bresson, B. Khelifa, and C. Mathieu, "The reflectivity spectra of Zn*X*P2 (*X*=Si, Ge, and Sn) compounds," J. Solid State. Chem. 177(11), 3859-3867 (2004). http://dx.doi.org/10.1016/j.jssc.2004.07.020
[9] B. Kocak and Y.O. Ciftci, *"Ab-initio* calculations of semiconductor," Mater. Res. Bull. 77, 300-306 (2016).https://doi.org/10.1016/j.materresbull.2016.02.008
[10] Y. Marfaing, "Énergie photovoltaïque," J. Phys. IV France, 12, Pr 2 – 145 (2002). https://doi.org/10.1051/jp420020021
[11] J. Müller, J. Nowoczin, and H. Schimitt, "Composition, structure and optical properties of sputtered thin films of CuInSe2,"Thin Solid Films, 496, 364-370 (2006).https://doi.org/10.1016/j.tsf.2005.09.077
[12] R.C. Gupta, P. Varshney, Pravesh, M. Lal, D. Kumar, K. Singh, and A.S. Verma, "Mechanical stability parameters ofchalcogenides and pnictides based optoelectronic materials," Chalcogenide Letters, 20(2), 101–112 (2023).https://doi.org/10.15251/CL.2023.202.101
[13] Suqin Xyue et al, The Electronic Structure and Optical Properties of $CdGeAs_2$ Crystal: A DFT and HSE06 Study, Materials and Surface Treatment Processes Used for Engineering Applications), Vol *12*(11), 1778 (2022). https://doi.org/10.3390/coatings12111778
[14] Aspnes (d. e.) and Cardona (m.) phys. rev.,, 173, 714.(1968). https://doi.org/10.1016/0022-3697(70)90234-9.
[15] Seraphin (b. 0.) and hess (r. b.), phys. rev. lett., , 14, 138. (1965). https://doi.org/10.1103/PhysRevLett.14.138.
[16] Burstein (e.), phys. rev., ,93, 632. (1954). https://doi.org/10.1103/PhysRev.93.632.
[17] Mengqiu Yu et al , Structural, electronic and optical properties of CdGeAs2 with hybrid density functional (HSE06), Materials Today Communications 31(1-3):103276 (2022). https://doi.org/10.1016/j.jallcom.2019.153610.
[18] You Yu et al , Ab initio study of the linear and nonlinear optical properties of chalcopyrite CdGeAs 2, Journal of Solid State Chemistry 185(12) (2012). https://doi.org/ .
[19] Madsen G. K. H., Blaha P., Schwarz K., Sjostedt E., Nordstr€om L., Phys. Rev. B 64, 195134 (2001); https://doi.org/10.1103/PhysRevB.64.195134
[20] Schwarz K., Blaha P., Madsen G. K. H., Comput. Phys. Commun. 147, 71 (2002); https://doi.org/10.1016/S0010-4655(02)00206-0
[21] Wu Z., Cohen R. E., Phys. Rev. B 73, 235116 (2006); https://doi.org/10.1103/PhysRevB.73.235116
[22] Tran F., Laskowski R., Blaha P., Schwarz K., Phys. Rev. B 75, 115131(2007); https://doi.org/10.1103/PhysRevB.75.115131
[23] Tran F., Blaha P., Phys. Rev. Lett. 102, 226401 (2009); https://doi.org/10.1103/PhysRevLett.102.226401
[24] Murnaghan F. D., Proc. Natl Acad. Sci. USA 30, 244 (1944); https://doi.org/10.1073/pnas.30.9.244
[25] Touat D., Ferhat M., Zaoui A., J. Phys.: Condens. Matter 18, 3647 (2006); https://doi.org/10.1088/0953-8984/18/15/011
[26] Xia H., Xia Q., Ruoff A. L., J. Appl. Phys. 74, 1660 (1993); https://doi.org/10.1063/1.354817
[27] Vegard L. Z., Phys. 5, 17 (1921); https://doi.org/10.1007/BF01349680
[28] Perri J. A., Laplaca S., Post B Acta Crystallography. 11, 310 (1958); https://doi.org/10.1107/S0365110X58000827

[29] Ku S. M., J. Electrochem. Soc. 113, 813 (1966); https://doi.org/10.1149/1.2424125
[30] Geisz J. F., Friedman D. J., Olson J., Kurtz M., Sarah R., Reedy R. C., Swartzlander A. B., Keyes B. M., Norman A. G., Applied Physics Letters 76(11), 1443 (2000); https://doi.org/10.1063/1.126058
[31] Archer R. J., Koyama R. Y., Loebner E. E., Lucas R. C., Phys. Rev. Lett. 12, 538 (1964); https://doi.org/10.1103/PhysRevLett.12.538
[32] Fomichev V. A., Zhukova I. I., Polushina I. K., J. Phys. Chem. Solids 29, 1025 (1968); https://doi.org/10.1016/0022-3697(68)90238-2
[33] Benchehima M., Abid H., Benchikh K., Mater. Chem. Phys. 198, 214 (2017); https://doi.org/10.1016/j.matchemphys.2017.06.009
[34] Tran F., Blaha P., Phys. Rev. Lett. 102, 226401 (2009); https://doi.org/10.1103/PhysRevLett.102.226401
[35] Charifi Z., Baaziz H., Bouarissa N., Int. J. Mod. Phys. B 18, 137 (2004); https://doi.org/10.1142/S0217979204023696
[36] Ravindra N. M. et al., Infrared Phys. Technol. 50, 21 (2007); https://doi.org/10.1016/j.infrared.2006.04.001
[37] Moss T. S., Proc. Phys. Soc. B 63, 167 (1950);https://doi.org/10.1088/0370-1301/63/3/302
[38] F. Wooten, *Optical Properties of Solids*, (Academic Press, New York and London, 1972). https://doi.org/10.1016/0169-4332(90)90007-M
[38] A. Ghosh, R. Thangavel, and M. Rajagopalan, "Electronic and optical modeling of solar cell compound CuXY2 (X = In, Ga, Al;Y = S, Se, Te): first-principles study via Tran–Blaha-modified Becke–Johnson exchange," J. Mater. Sci. 50, 1710-1717 (2015). http://dx.doi.org/10.1007/s10853-014-8732-z
[39] J.T. Goldstein, D.E. Zelmon, A.W. Saxler, S.M. Hegde, J.D. Wolf, P.G. Schunemann, et al., "Infrared properties of a nonlinear optical chalcopyrite semiconductor," J. Appl. Phys. 86, 94 (1999). http://dx.doi.org/10.1063/1.370704
[40] P.A. Franken, A.E. Hill, C.W. Peters, and G. Weinreich, "Generation of optical harmonics," Phys. Rev. Lett. 7, 118 (1961). https://doi.org/10.1103/PhysRevLett.7.118
[41] H. Salehi, and E. Gordanian, "Ab initio study of structural, electronic and optical properties of ternary chalcopyrites emiconductors," Mat. Sci. Semicon. Proc. 47, 51-56 (2016). https://doi.org/10.1016/j.mssp.2016.02.015.
[42] R.R. Reddy, Y.N. Ahammed, K.R. Gopal, and D.V. Raghuram, "Optical electronegativity and refractive index of materials,"Opt. Mater. 10(2), 95-100 (1998). https://doi.org/10.1016/S0925-3467(97)00171-7.
[43] S. Cui, W. Feng, H. Hu, Z. Feng, and Y. Wang, "First principles studies of phase stability, electronic and elastic properties, computational Materials Science," 47(4), 968-972 (2010). https://doi.org/10.1016/j.commatsci.2009.11.030.